Original Article

Quantitative Analysis of Image Quality in Low-Dose Computed Tomography Imaging for COVID-19 Patients

Behrooz Ghane[1], Alireza Karimian[1], Samaneh Mostafapour[2], Faezeh Gholamiankhak[3], Seyedjafar Shojaerazavi[4], Hossein Arabi[5]

[1]Department of Biomedical Engineering, Faculty of Engineering, University of Isfahan, Isfahan, [2]Department of Radiology Technology, Faculty of Paramedical Sciences, Mashhad University of Medical Sciences, [4]Department of Cardiology, Ghaem Hospital Mashhad, Mashhad University of Medical Sciences, Mashhad, [3]Department of Medical Physics, Faculty of Medicine, Shahid Sadoughi University of Medical Sciences, Yazd, Iran, [5]Division of Nuclear Medicine and Molecular Imaging, Geneva University Hospital, Geneva, Switzerland

Abstract

Background: Computed tomography (CT) scan is one of the main tools to diagnose and grade COVID-19 progression. To avoid the side effects of CT imaging, low-dose CT imaging is of crucial importance to reduce population absorbed dose. However, this approach introduces considerable noise levels in CT images. **Methods:** In this light, we set out to simulate four reduced dose levels (60% dose, 40% dose, 20% dose, and 10% dose) of standard CT imaging using Beer–Lambert's law across 49 patients infected with COVID-19. Then, three denoising filters, namely Gaussian, bilateral, and median, were applied to the different low-dose CT images, the quality of which was assessed prior to and after the application of the various filters via calculation of peak signal-to-noise ratio, root mean square error (RMSE), structural similarity index measure, and relative CT-value bias, separately for the lung tissue and whole body. **Results:** The quantitative evaluation indicated that 10%-dose CT images have inferior quality (with RMSE = 322.1 ± 104.0 HU and bias = 11.44% ± 4.49% in the lung) even after the application of the denoising filters. The bilateral filter exhibited superior performance to suppress the noise and recover the underlying signals in low-dose CT images compared to the other denoising techniques. The bilateral filter led to RMSE and bias of 100.21 ± 16.47 HU and − 0.21% ± 1.20%, respectively, in the lung regions for 20%-dose CT images compared to the Gaussian filter with RMSE = 103.46 ± 15.70 HU and bias = 1.02% ± 1.68% and median filter with RMSE = 129.60 ± 18.09 HU and bias = −6.15% ± 2.24%. **Conclusions:** The 20%-dose CT imaging followed by the bilateral filtering introduced a reasonable compromise between image quality and patient dose reduction.

Keywords: *COVID-19, denoising filters, image quality, low-dose computed tomography, patient dose*

Submitted: 16-Nov-2021 **Revised:** 31-Dec-2021 **Accepted:** 19-Apr-2022 **Published:** 29-May-2023

Introduction

The World Health Organization identified severe acute respiratory syndrome (SARS) coronavirus 2, which causes a SARS, as a global public health concern.[1] Up to this date (November 07, 2021), more than 250 million cases have been diagnosed with coronavirus disease.[2] Coronavirus or COVID-19 affects the respiratory system and causes mild-to-severe respiratory syndromes, including pneumonia. The management, outbreak prevention, and treatment of this disease are currently the most critical global challenges in medicine.[3,4] Therefore, an accurate and quick diagnosis of this disease is of essential importance. Real-time reverse transcription-polymerase chain reaction (RT-PCR) test is regarded as a standard method for the diagnosis of COVID-19. However, this method has severe limitations such as the preparation time, considerable false-positive and false-negative rates,[5] and relatively low sensitivity.[6] Preliminary studies have confirmed that computed tomography (CT) imaging is an effective approach for diagnosing COVID-19 disease.[7,8] CT imaging is an accurate and noninvasive method for detecting abnormalities, including tumors, bone fractures, and cardiovascular diseases.[9-12] Recently, an extended range of clinical studies has been performed on the potentials of CT imaging for the diagnosis and management of patients with COVID-19 disease. These studies, in fact, continue to fully identify the underlying COVID-19 features in CT images.[8,13]

How to cite this article: Ghane B, Karimian A, Mostafapour S, Gholamiankhak F, Shojaerazavi S, Arabi H. Quantitative analysis of image quality in low-dose computed tomography imaging for COVID-19 patients. J Med Sign Sens 2023;13:118-28.

Address for correspondence:
Prof. Alireza Karimian, Department of Biomedical Engineering, Faculty of Engineering, University of Isfahan, Isfahan, Iran.
E-mail: karimian@eng.ui.ac.ir

Access this article online

Website: www.jmssjournal.net

DOI: 10.4103/jmss.jmss_173_21

Quick Response Code:

Although CT imaging is a rapid method for the diagnosis of COVID-19 disease, the absorbed radiation dose by patients, due to the X-ray exposure, is one of its major concerns.[14] The radiation risks of CT scans are seriously high for those required to undergo multiple scans, pregnant women, and pediatrics.[15] A recent study showed that DNA double-strand breaks and chromosome aberrations would increase in patients who undergo standard-dose CT scans, while there was no DNA damage in people who have been examined with low-dose CT scans.[16] Despite the significant advances made in software and hardware technology of CT scanners,[17,18] it is not yet considered a low-dose safe imaging modality.[19] Therefore, regarding CT scan's side effects,[20] the application of low-dose CT protocols would be of crucial importance in routine CT imaging. However, increased image noise is a major limitation in this imaging modality.[21]

The diagnosis of COVID-19 (infection) patterns within the lung region would be highly challenging in CT images with increased noise levels, which can skew the correct diagnosis. Reducing noise levels in CT images and enhancing the image quality have always been one of the important research topics.[22,23]

Noise reduction in low-dose CT imaging can be achieved in three ways:[24] denoising in the sinogram or projection space prior to the image reconstruction,[25,26] using the dedicated reconstruction algorithms which model the noise within image formation,[27,28] and denoising in the image domain using postreconstruction algorithms.[21,29] For instance, Wang *et al*. represented suppression noise-induced streak artifacts and preserving resolution in the reconstructed images that may have advantage in low-dose CT imaging.[30] A study of Thibault *et al*. showed that Bayesian iterative algorithms significantly improve the quality of CT images.[31] The other study for noise reduction in low-dose CT scan images was reported by Karimi *et al.* They proposed a denoising algorithm that was based on maximizing the data likelihood and sparsity in the gradient domain. The proposed algorithm was applied to the projection data and significantly reduced the noise in low-dose CT.[32] The induced noise in low-dose CT images normally follows a Poisson noise distribution, Gaussian noise distribution, or a combination of the two.[33] The commonly used denoising techniques in medical imaging are Gaussian, median, and bilateral filters which could be employed either in the projection or image space.[34,35] Implementation of these techniques in the projection space requires access to the raw acquisition data which is not commonly provided by CT scanners.[24] Iterative CT image reconstruction algorithms tend to model the underlying causes of noise within the image reconstruction process to suppress the noise in the resulting images, commonly through the maximum likelihood formulation of the Poisson noise. The advantage of iterative reconstruction techniques is noise statistics at projection data which can be considered into account during the reconstruction process directly. However, these techniques, in addition to high computation time, also require raw acquisition data. Moreover, they should be dedicatedly developed/optimized for each scanner and acquisition protocol to properly perform noise suppression.[24,36,37]

The denoising techniques in the image domain, contrary to the other approaches, do not require raw sinogram data and can directly be applied to CT images. In addition to low computation time, these techniques are almost independent of CT scanners, acquisition protocols, and image reconstruction algorithms. Moreover, they could easily be adapted to the new acquisition protocols and, or noise levels through the adjustment of a few parameters. Sadri *et al*. provided a two-stage approach to remove the impulse noise in medical images. In their method, first, impulse noise was detected by wavelet network and then removed by using median filter.[38] Manduca *et al*. demonstrated that bilateral filtering, which smooths values based on weighted average in the local neighborhood, can improve the image quality in CT scan. Results showed that this method can reduce the noise better than commercial reconstruction kernels.[34] Kim *et al*. proposed a fast nonlocal means (FNLM) algorithm. This algorithm suppressed the noise in low-dose CT images while would preserve the edge information. They used image processing filters such as Gaussian, median, and Weiner that were applied to MASH noisy phantom and compared with FNLM algorithm. This study presented FNLM denoising that can reduce noise in thoracic CT images.[39]

In addition to the above-mentioned approaches, deep learning-based denoising techniques have exhibited promising performance in low-dose CT imaging.[40,41] These methods require an extensive training dataset to create a robust model to intersubject image quality and, or anatomical variations. Moreover, these techniques are very sensitive to abnormal and, or odd cases wherein they may lead to gross errors and misdiagnosis.[21,42-45]

The aim of this work is to investigate low-dose CT imaging for COVID-19 patients, and in particular, how reduced patient dose would affect the quality of the CT images. To this end, the low-dose CT imaging of COVID-19 patients will be simulated for different dose levels up to 10% of the standard dose to measure the increased noise levels and quantitative bias. Thereafter, different postreconstruction denoising approaches, namely Gaussian, median, and bilateral filters, will be applied to the low-dose CT images to suppress the noise and recover the image quality. The goal is to determine which reduced dose level and postreconstruction denoising approach would lead to an optimal compromise between image quality and patient radiation dose.

Materials and Methods

Data acquisition

Chest CT scans from 49 patients with positive COVID-19 (approved by the RT-PCR test) were acquired between January and March of 2020 in Shariati Hospital, Mashhad, Iran. CT image acquisitions were then performed on a Siemens Somatom Spirit Dual Slice CT with tube energy of 130 kVp, tube current of 48 mAs, CT dose index ($CTDI_{VOL}$) of 5.64 mGy, dose–length product of 132.32 mGy. cm, rotation time (TI) of 0.8 s, and slice thickness of 5 mm. For the entire group of patients, the lung region was semi-automatically segmented from the standard CT images using Pulmonary Toolkit (PTK) software, London, England.[46] The lung segmentation was visually verified, and the miss-segmentation errors were manually corrected.

Low-dose computed tomography simulation

In this study, low-dose CT imaging was simulated for reduced doses of 60%, 40%, 20%, and 10% of the standard CT images (reference). To this end, the method proposed by Wang *et al.*[47] was employed to simulate low-dose CT imaging as described in the following steps.

The parallel beam geometry estimates the spatial coordinates of the X-ray beam passing through the subject in the field of view. Figure 1 depicts the concept of parallel beam geometry and its key parameters.

A single point in space is defined by a combination of φ and *s* parameters which are the angle between the X-ray beam and the distance of the X-ray beam from the center, respectively. Since the $L_{s,\varphi}$ line is perpendicular to the X-ray beam, it can be described by a point (x, y) on $L_{s,\varphi}$ using a real number $t \in \mathbb{R}$ and $\varphi \in (0,2\pi)$ as follows:

$$L_{s,\varphi}(t) = (x(t), y(t)) = s(\cos\varphi, \sin\varphi) + t(-\sin\varphi, \cos\varphi). \quad (1)$$

Then, function $f(L_{s,\varphi})$ can be defined on $\mathbb{R}^2$ as:

$$Rf(s,\varphi) = \int_{-\infty}^{+\infty} f\left(L_{s.\varphi}(t)\right)dt\,. \quad (2)$$

In the above equation, *R* is the Radon transform which is applied to the *f* function.

Based on Beer–Lambert's law, the result of applying the Radon transforms in Eq. 2 would be

$$Rf(s,\varphi) = -ln\left(\frac{I_1(s.\varphi)}{I_0(s.\varphi)}\right) = y(s,\varphi) \quad (3)$$

I_0 is the intensity at the X-ray source and I_1 is the intensity (signal) recorded in the detector.

According to Eq. 3, the added noise on the CT images could be modeled by a Poisson distribution as follows:

1. Eq. 4 calculates Hounsfield unit (HU) values (CT numbers) from the standard-dose CT images (reference), where *Intercept* and *Slope* values are obtained from DICOM header information.

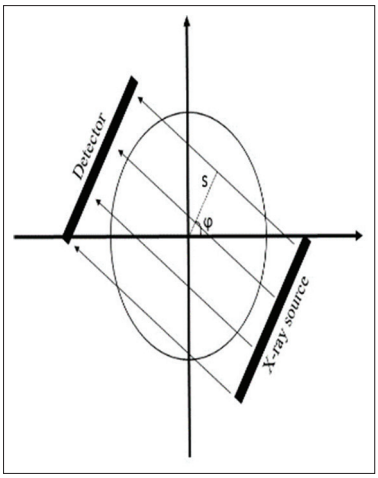

Figure 1: Parallel beam geometry and its key parameters

$$HU_s = (PixelValue \times Slope) + Intercept \quad (4)$$

2. Considering the tube voltage in standard CT imaging, we assume $\mu_{air} = 0$ and the linear attenuation coefficients were computed using Eq. 5

$$\mu_{tissue} = \left(HU_s \times \frac{\mu_{water}}{1000}\right) + \mu_{water} \quad (5)$$

3. The projection data (ρ_s) is obtained from the application of the Radon transform to the reference CT images (converted to the linear attenuation coefficients).
4. The normal-dose transmission data (T_{nd}) is calculated using Eq. 6

$$T_{nd} = exp(-\rho_s) \quad (6)$$

5. The low-dose transmission data (T_{ld}) is generated by adding Poisson noise to the original data

$$T_{ld} = Poisson(I_0 \times T_{nd}), \quad (7)$$

Where I_0 is the incident flux for simulating low-dose scans.

6. The low-dose projection data (ρ_{ld}) is calculated in the sinogram domain using Eq. 8

$$\rho_{ld} = ln\left(\frac{I_0}{T_{ld}}\right) \quad (8)$$

7. Finally, the inverse of Eq. 5 is applied to convert the attenuation coefficients to the CT values, and the final low-dose image is reconstructed using the inverse Radon transform and filter back-projection algorithm.

Based on Beer–Lambert's law, the intensity index I_0 indicates the number of photons per detector bin in the air scan, which is chosen 6000 for 60% low-dose simulation. According to Ref. 37, I_0 was assumed 10^4 in the full-dose imaging, thus $I_0 = 6000$ was considered 60% low-dose, $I_0 = 4000$ as 40%, $I_0 = 2000$ as 20%, and $I_0 = 1000$ as 10% low-dose CT imaging.

Denoising algorithms

Gaussian filter

Gaussian filter is a simple and intuitive approach of noise suppression that replaces the value of each pixel with the

weighted average of surrounding ones. This approach may introduce noticeable signal loss and blur in the CT images. The Gaussian filter is defined as

$$F(x, y) = \frac{1}{2\pi\sigma^2} e^{-\frac{x^2+y^2}{2\sigma^2}} \quad (9)$$

Where x and y are the vertical and horizontal distances from the target pixel (in two-dimensional implementation) and σ is the standard deviation of the Gaussian distribution. The kernel obtained from this equation is convolved with the noisy CT images to diminish the noise levels. The standard deviation of the Gaussian kernel is the key parameter that defines the levels of smoothness in the resulting images. The procedure to find optimal standard deviation values for the different noise levels (low-dose CT images) is described in the following section.

Median filter

The median filter, as a nonlinear denoising approach, is commonly used for noise suppression in natural as well as medical images. The median filter is functionally similar to the moving average filter, but it calculates the median value of the pixels/voxels rather than the mean value. Median filters might exhibit better performance regarding the edge preservation in the filtered images than the Gaussian filter. The median filter is formulated as

$$F(x, y) = median(x, y). \quad (10)$$

Where $x \times y$ defines the size of the filter window for calculation of the median value. The filter window size should be optimized independently for the different low-dose CT images.

Bilateral filter

Bilateral filter, regarded as an edge-preserving smoothing approach, tends to suppress noise while maintaining the prominent edges/patterns of the image through penalizing the smoothing function over the edges.[48] The bilateral filter, employed to reduce the noise levels in the different low-dose CT images, is mathematically formulated as

$$w(i, j, k, l) = exp\left(-\frac{(i-k)^2+(j-l)^2}{2\sigma_d^2} - \frac{\|I(i,j)-I(k,l)\|^2}{2\sigma_r^2}\right) \quad (11)$$

Here, *(i, j)* and *(k, l)* indicate the location of the target voxel to be filtered as well as its neighboring voxels. *w (i, j, k, l)* returns the weighting factors for each of the neighboring voxels *(k, l)* based on spatial closeness (first term in Eq. 11) and intensity difference (second term in Eq. 11) with respect to the target voxel *(i, j)*. *I (i, j)* and *I (k, l)* denote the intensity of *(i, j)* and *(k, l)* voxels, respectively, and σ_d and σ_r are the smoothing parameters. The calculated weights from Eq. 11 are used in Eq. 12 to estimate the noise-free voxel values (I_D) in the filtered images.

$$I_D(i, j) = \frac{\sum_{k,l} I(k,l) w(i,j,k,l)}{\sum_{k,l} w(i,j,k,l)} \quad (12)$$

Quantitative evaluation

The performance of the Gaussian, median, and bilateral denoising techniques was evaluated on the CT images with different dose levels using the following four image quality metrics.

Peak signal-to-noise ratio (PSNR) presents the ratio between the maximum intensity of the noisy or reference image and the mean square error (MSE), which is usually expressed in the unit of logarithmic decibel as follows:

$$PSNR(y, x) = 10\log_{10}\left(\frac{max(x)^2}{MSE(y, x)}\right) \quad (13)$$

Here, x is the full-dose CT image (reference), y is the low-dose (or filtered) CT image, and *MSE (y, x)* stands for the mean squared error between the reference and low-dose (filtered) CT images as follows:

$$MSE = \frac{1}{mn}\sum_{i=0}^{m-1}\sum_{j=0}^{n-1}[x(i,j)-y(i,j)]^2 \quad (14)$$

Here, m × n (row × column) is the number of voxels in the CT images and i and j stand for the voxel indices.

Structural similarity index measure (SSIM), which reflects the perceived quality of the images, was used to compare the overall structural similarity between the low-dose (or filtered) and reference CT images.

$$SSIM(x, y) = \frac{(2\mu_x\mu_y + c_1)(2\sigma_{xy} + c_2)}{(\mu_x^2 + \mu_y^2 + c_1)(\sigma_x^2 + \sigma_y^2 + c_2)} \quad (15)$$

Here, x is the full-dose CT image (reference), y indicates the low-dose (or filtered) CT image, and μ_x and μ_y are the mean intensity values of the x and y images, respectively. Similarly, σ_x^2 and σ_y^2 are the variance of the x and y images, respectively, and σ_{xy} stands for the covariance of x and y. Constants c_1 and c_2 are utilized to avoid division by zero (or very small numbers).

Root MSE (RMSE) measures the difference between CT values in the noisy and reference CT images.

$$RMSE = \sqrt{MSE} \quad (16)$$

MSE was defined in Eq. 14.

Relative bias *(BAIS)* indicates the percentage of error in the low-dose or filtered CT images with respect to the reference CT images.

$$BIAS = \left(\frac{y-x}{x}\right) \times 100 \quad (17)$$

Here, x and y denote the CT values in the full-dose and low-dose CT images, respectively.

One of the major challenges in the application of the postreconstruction denoising techniques is finding the optimal values for the parameters to achieve the best image quality. Optimal sets of the parameters would lead to maximal PSNR and SSIM indices as well as minimum RMSE and BIAS. To optimize the parameters of the Gaussian, median, and bilateral filters, a reasonably wide

range of values were set for these parameters, and the ones leading to the maximum PSNR and minimum RMSE were selected for the final implementation of these filters. In fact, our goal in this section is to find the optimal value of the parameter and not its best case. In other words, our goal is not to get the best parameter for each image but to find an approximate parameter that is comprehensive for all images. For this purpose, we approximated the optimal parameter value for the other images too. It should be noted that this procedure was repeated independently for each level of the low-dose CT images. Figure 2 shows a representative example of this optimization procedure for the Gaussian parameter at the low-dose level of 60% which is related to one patient. This procedure was performed randomly for 5 patients at four dose levels and all filters. Then, the mean of the obtained parameter value in each section was selected as the optimal parameter. Finally, the relevant filter was applied to all patients using these optimal parameters. The BIAS, PSNR, and RMSE metrics were calculated for the whole body, lung, and whole body without lung, separately.

Results

Figure 3 depicts the simulated low-dose CT images at 60%, 40%, 20%, and 10% of the standard-dose levels for a representative patient with positive COVID-19 test. The quantitative metrics, including SSIM, PSNR, RMSE, and BIAS, calculated for the different low-dose CT images within the whole body, lung, and whole body without lung, are reported in Table 1.

Table 2 presents the quantitative metrics calculated after the application of the Gaussian filter to the different low-dose CT images. The SSIM and PSNR indices increased after the application of the Gaussian filters, which indicates the overall improved quality of the resulting images. Figure 4 presents the low-dose CT images after the application of the Gaussian filter [for the same views presented in Figure 2]. Visual inspection revealed effective noise reduction; however, some streak-like artifacts are seen in the 10% low-dose image.

Table 3 summarizes the evaluation parameters calculated for the different low-dose CT images after the application of the median filter. Compared to the Gaussian filter, the median filter led to noticeable signal loss, particularly in 10% low-dose CT images with more than -9% bias in the lung region. Overall, the median filter exhibited inferior performance compared to the Gaussian filter with increased RMSE and reduced SSIM. Figure 5 displays the median filtered low-dose CT images wherein less effective noise reduction is observed compared to the Gaussian filtered images in Figure 4.

Similarly, the quantitative evaluation of the bilateral filtering in terms of PSNR, SSIM, RMSE, and BIAS parameters is reported in Table 4, wherein reduced quantitative bias and improved SSIM and PSNR are observed compared

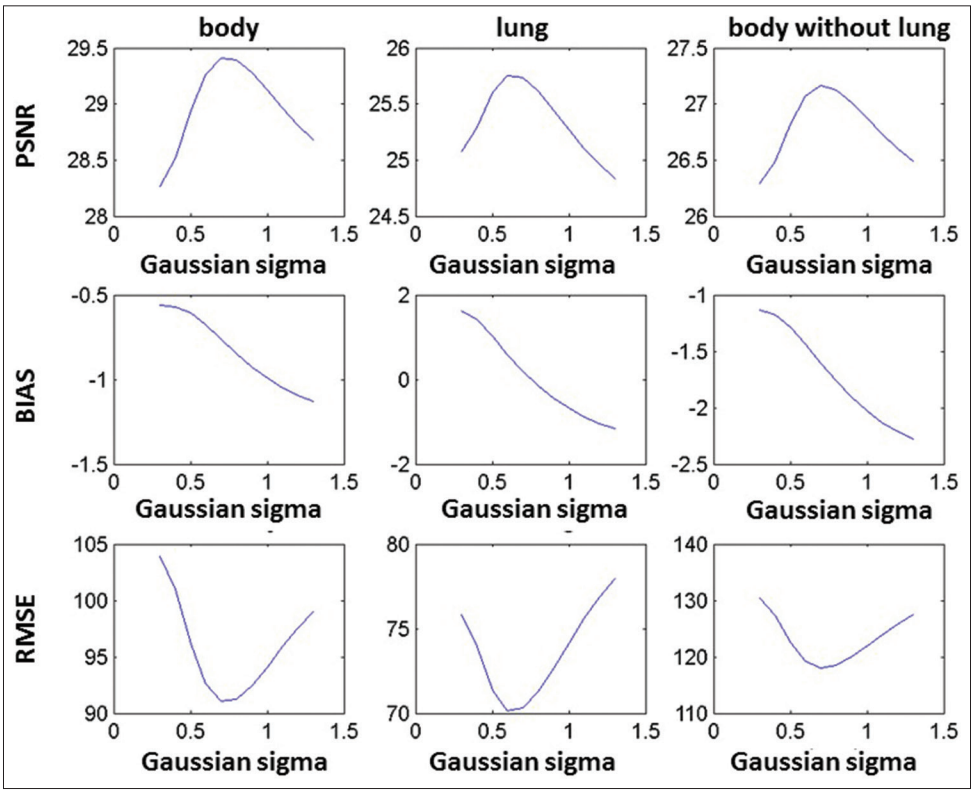

Figure 2: The optimal value achieved for the Gaussian parameter (sigma) at the low-dose level of 60% for a patient. This procedure is performed the same for all four dose levels. RMSE – Root mean square error; PSNR – Peak signal-to-noise ratio

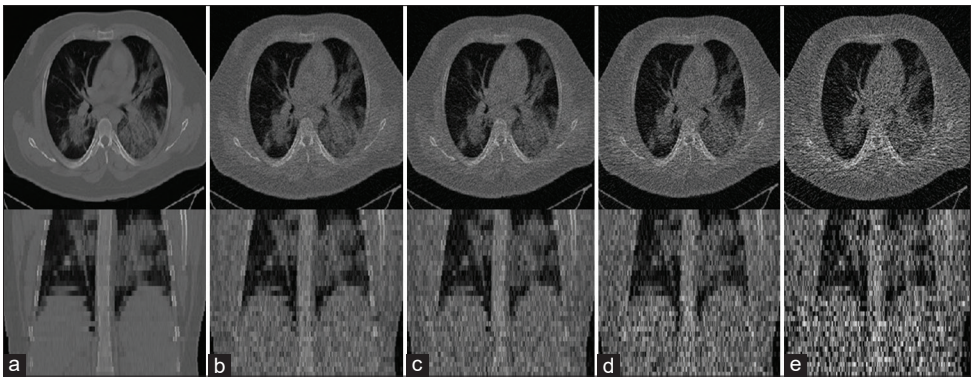

Figure 3: Simulated low-dose CT images for a representative patient with positive COVID-19 test. (a) Reference CT image (full dose). (b) 60% of full dose. (c) 40% of full dose. (d) 20% of full dose. (e) 10% of full dose. CT – Computed tomography

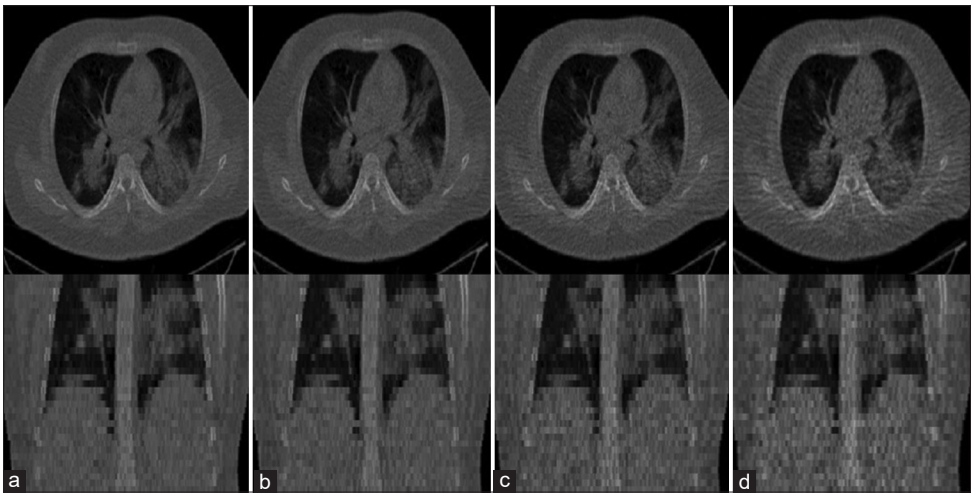

Figure 4: (a) 60% low-dose, (b) 40% low-dose, (c) 20% low-dose, and (d) 10% low-dose CT images after application of the Gaussian filter. CT – Computed tomography

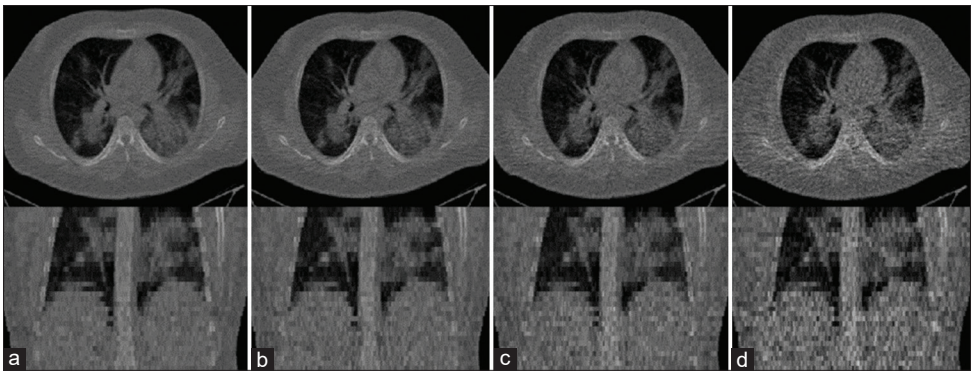

Figure 5: (a) 60% low-dose, (b) 40% low-dose, (c) 20% low-dose, and (d) 10% low-dose CT images after application of the median filter. CT – Computed tomography

to the Gaussian and median filters. The bilateral filtering led to a maximum bias of <5% compared to the Gaussian and median filters with a bias of more than 7% and -9%, respectively. Figure 6 illustrates the effective noise reduction in the bilateral filtered images, particularly in the 20% low-dose CT image, wherein the pattern of infection can be clearly seen in the lung region with minimal signal loss and, or artifact.

To compare the performance of the different denoising techniques for the different low-dose levels, boxplots of the RMSE and BIAS parameters are presented in Figure 7. It is clearly seen that the bilateral filter resulted in noticeably lower BIAS and RMSE in the four low-dose CT images within the lung region. Although the bilateral filter enabled remarkable noise reduction, the BIAS in the 10% low-dose CT images within the lung region is yet significantly high,

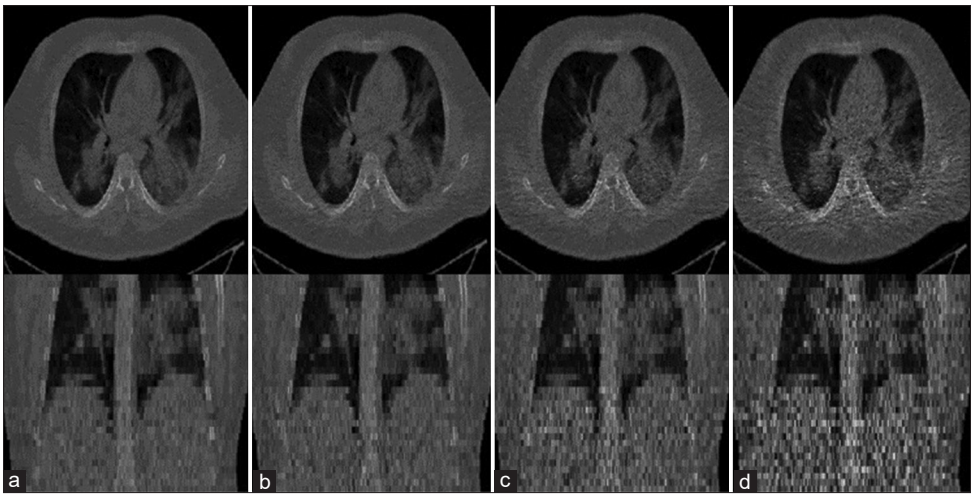

Figure 6: (a) 60% low-dose, (b) 40% low-dose, (c) 20% low-dose, and (d) 10% low-dose CT images after application of the bilateral filter. CT – Computed tomography

Table 1: Mean±standard deviation of peak signal-to-noise ratio, structural similarity index measure, root mean square error, and bias metrics calculated for the different low-dose computed tomography within the whole body, lung, and whole body without lung across 49 patients

	SSIM	PSNR	RMSE (HU)	Bias (%)
60% dose				
Whole body	0.64±0.09	26.64±2.14	152.91±27.08	−0.10±0.23
Lung	0.93±0.02	23.57±2.17	124.25±27.96	1.50±0.69
Whole body without lung	0.71±0.09	26.17±2.07	160.97±25.49	−0.14±0.25
40% dose				
Whole body	0.59±0.10	24.66±2.20	191.80±38.23	0.18±0.31
Lung	0.92±0.02	21.95±2.30	151.10±37.32	1.99±0.93
Whole body without lung	0.68±0.09	24.16±2.1	202.63±36.64	0.14±0.32
20% dose				
Whole body	0.53±0.11	20.90±2.38	297.41±68.05	1.26±0.71
Lung	0.90±0.02	18.89±2.59	217.37±64.66	4.30±1.85
Whole body without lung	0.63±0.10	20.33±2.29	316.46±66.43	1.17±0.70
10% dose				
Whole body	0.47±0.11	17.22±2.33	452.90±94.95	4.09±1.75
Lung	0.85±0.02	15.54±2.78	322.08±103.99	11.44±4.49
Whole body without lung	0.58±0.10	16.62±2.21	483.14±89.84	3.78±1.63

SSIM – Structural similarity index measure; PSNR – Peak signal-to-noise ratio; RMSE – Root mean square error; HU – Hounsfield unit

which might skew the correct diagnosis of the infection in the lung region. To fairer comparisons, analysis of variance test was applied to evaluate the lung RMSE values for these three filters. According to this test, *P* value result was compared between bilateral, median, and Gaussian filters, which indicates that the bilateral filter performs the noise removal operation significantly better than other filters ($P < 0.00001$).

Discussion

In this work, four different low-dose CT imaging, namely 10%, 20%, 40%, and 60% of the standard dose, were simulated for a group of COVID-19 patients. The aim of this study was to investigate to what extent low-dose imaging would deteriorate the quality of CT images for COVID-19 patients and how postreconstruction filtering could recover the missing signals and underlying structures. Since COVID-19 disease causes infection in the lung, noise levels in this region were separately assessed before and after applying the various denoising techniques.

Based on complications of CT scan and As Low As Reasonably Achievable principle, especially in children and multiple imaging in some patients during diagnosis or treatment process,[49] firstly, we simulated four levels of dose and, secondly, demonstrated that dose can be reduced to 20% or one-fifth of the standard dose and then image quality can improve up close to the original image using bilateral filter for clinical evaluation.

Regarding Figure 7, dose reduction in CT imaging up to 60% and 40% of the standard dose would not cause a remarkable noise rise in the lung region, wherein quantitative bias of <2% was observed. On the other hand, the noise levels increased dramatically in the 20% and 10% low-dose images, causing more than 4% and 11% quantitative bias in the lung region, respectively. Although the bilateral filter was able to reduce quantitative bias in the lung region up to -0.21% for 20%-dose and 4.91% for 10%-dose imaging, noticeable streak-like artifacts were observed over the COVID-19 infections within the lung, particularly in 10%-dose images. These image artifacts might skew the accurate diagnosis of COVID-19 and, or identifying or grading the infection in the lung. Thus, 10%-dose imaging, even after the application of the bilateral filter, would not be a reasonable option for the diagnosis of COVID-19 patients.

Table 2: Mean±standard deviation of peak signal-to-noise ratio, structural similarity index measure, root mean square error, and bias calculated for the different low-dose computed tomography after application of the Gaussian filter within the whole body, lung, and whole body without lung across 49 patients

	SSIM	PSNR	RMSE	Bias
60% dose				
Whole body	0.74±0.06	30.97±1.84	91.30±6.40	−0.51±0.39
Lung	0.93±0.01	26.62±1.43	86.36±9.73	−1.29±0.52
Whole body without lung	0.78±0.09	28.97±1.99	115.15±10.96	−1.47±0.62
40% dose				
Whole body	0.72±0.07	30.13±1.79	100.66±8.08	−0.23±0.47
Lung	0.93±0.01	26.10±1.50	91.82±11.77	−0.80±0.75
Whole body without lung	0.77±0.06	28.34±1.86	123.72±9.48	−1.19±0.70
20% dose				
Whole body	0.69±0.08	28.61±1.82	120.20±12.97	0.75±0.90
Lung	0.93±0.01	25.09±1.60	103.46±15.70	1.02±1.68
Whole body without lung	0.78±0.07	27.04±1.79	143.5±10.93	−0.40±1.12
10% dose				
Whole body	0.66±0.08	26.51±1.93	153.60±21.12	3.48±1.96
Lung	0.90±0.02	23.43±1.89	126.08±25.1 0	7.70±4.33
Whole body without lung	0.71±0.07	25.27±1.80	176.34±15.90	2.01±2.07

SSIM – Structural similarity index measure; PSNR – Peak signal-to-noise ratio; RMSE – Root mean square error

Table 3: Mean±standard deviation of peak signal-to-noise ratio, structural similarity index measure, root mean square error, and bias calculated for the different low-dose computed tomography after application of the median filter within the whole body, lung, and whole body without lung across 49 patients

	SSIM	PSNR	RMSE	Bias
60% dose				
Whole body	0.71±0.07	30.79±1.79	93.27±7.26	−0.60±0.37
Lung	0.93±0.01	26.21±1.50	90.44±9.60	−1.99±0.77
Whole body without lung	0.77±0.07	29.94±1.81	102.85±8.55	−0.75±0.38
40% dose				
Whole body	0.67±0.08	29.70±1.81	105.96±10.86	−0.43±0.44
Lung	0.93±0.02	25.36±1.61	99.98±13.11	−2.32±0.96
Whole body without lung	0.74±0.07	28.87±1.78	116.41±10.75	−0.55±0.44
20% dose				
Whole body	0.63±0.09	28.09±1.81	127.42±11.55	−0.28±0.80
Lung	0.91±0.03	23.12±1.62	129.60±18.09	−6.15±2.24
Whole body without lung	0.72±0.09	25.52±2.09	171.97±21.43	−1.19±1.81
10% dose				
Whole body	0.55±0.10	25.92±1.88	163.86±18.02	1.00±1.40
Lung	0.86±0.04	21.61±1.85	155.10±27.90	−9.16±4.02
Whole body without lung	0.66±0.09	23.47±2.04	217.63±25.04	0.04±1.69

SSIM – Structural similarity index measure; PSNR – Peak signal-to-noise ratio; RMSE – Root mean square error

One of the most important issues in CT imaging of COVID-19 patients is the diagnosis, grading, and classification of the infection in the lung region. In this regard, it is essential to preserve the underlying structures and patterns of the lung region within low-dose imaging and postreconstruction noise suppression. Hilts and Duzenli[35] concluded that the simple moving average filtering would be able to effectively suppress the noise in low-dose CT imaging; however, the noticeable loss of signals and structures in the resulting images, particularly in the lung region, greatly limits its application for COVID-19 patients. Thanh and Surya[50] demonstrated that parameter optimization for the bilateral filter is challenging as the optimal values may vary across the subjects due to different noise levels and, or underlying structures. However, in this study, the lung region was not dedicatedly investigated to relate the findings to the COVID-19 CT imaging.

In this work, the lung segmentation algorithm implemented in the PTK package was used for the delineation of the lung region. Alnaser *et al*. compared the PTK approach with four different algorithms for the segmentation of the lung, which demonstrated the superior performance of the PTK algorithm.[46] Although the dataset in this study contained challenging lung parenchyma tissues due to the presence of COVID-19 infection, the automated lung segmentation exhibited acceptable accuracy, wherein slight miss-classification errors were manually corrected.

Optimization of the parameters is the key to the efficient performance of different denoising techniques. To this end, the parameters of each filter were separately optimized for each dose level. An ideal denoising algorithm would lead to zero quantitative bias and RMSE with respect to the reference images. As such, the parameters which resulted in minimum RMSE or BIAS, as well as maximum PSNR, were selected dedicatedly for each dose level and denoising technique. It should also be mentioned that the levels of noise presented in the simulated low-dose CT images depend on the CT scanner, acquisition protocol, as well as the resolution of the CT images. Therefore, the optimization of these parameters should be repeated when the input CT images are from different scanners or acquired through the use of different acquisition protocols.

Overall, considering Figure 7, the bilateral filter led to a noticeable smaller quantitative bias and RMSE compared to the other denoising techniques, regardless of the noise levels in the input images. The quantitative bias observed in the bilateral filtered images was <5% even in 10%-dose images, which is a clinically tolerable error. However, due

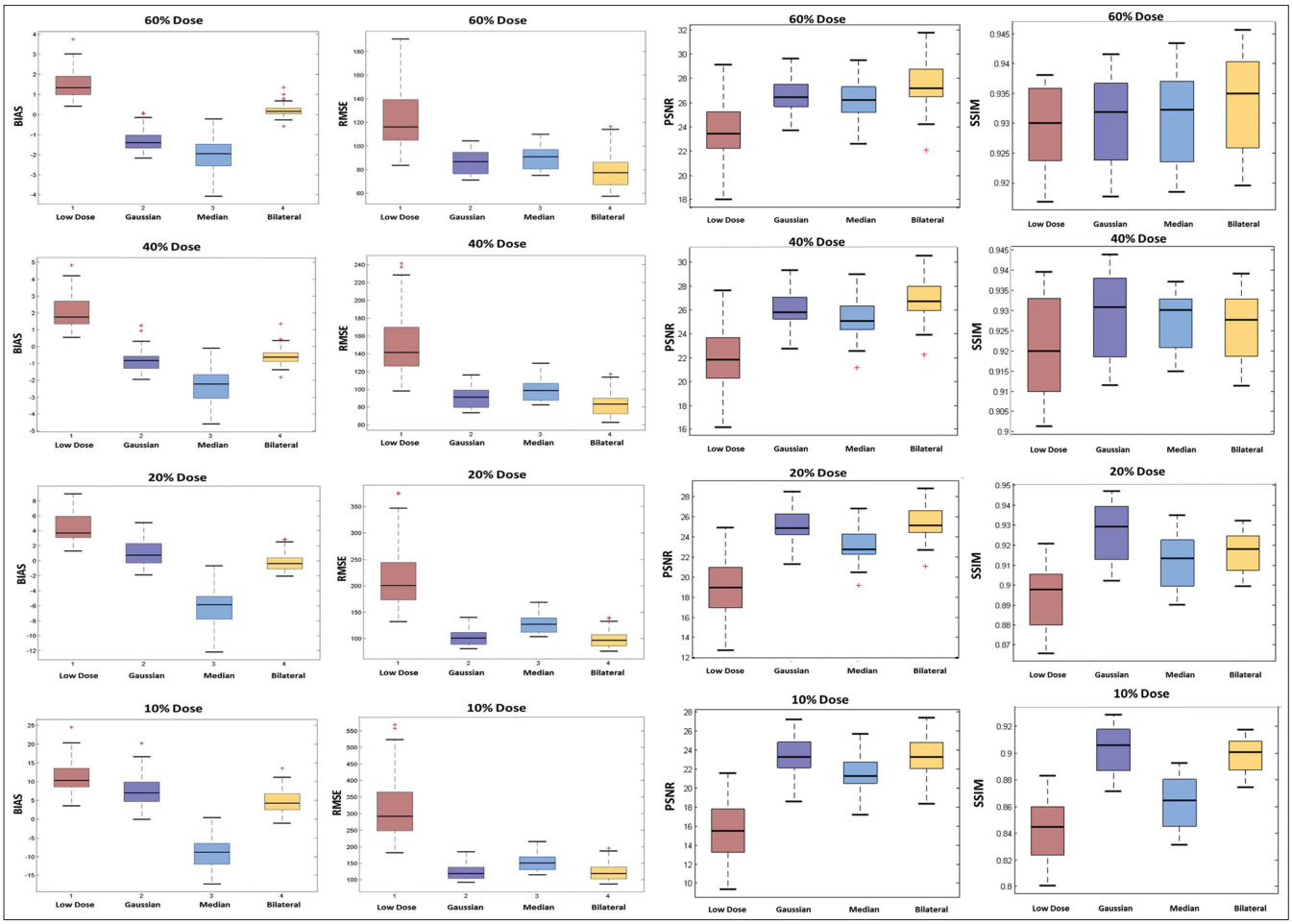

Figure 7: Boxplots of BIAS (%), RMSE (HU), PSNR (HU), and SSIM metrics calculated for the different denoising techniques and the different low-dose levels within the lung region. RMSE – Root mean square error; HU – Hounsfield unit; PSNR – Peak signal-to-noise ratio; SSIM – Structural similarity index measure

to the presence of the streak-like artifacts in the lung, which might skew the correct classification of the COVID-19 infection, 10%-dose imaging is not recommended even after bilateral filtering. On the other hand, 20%-dose CT imaging would offer an acceptable compromise between dose reduction and image quality wherein the quantitative bias in the lung region did not exceed 5% and -1% before and after the application of the bilateral filter.

Regarding the quantitative errors in the lung region and the image artifacts, which might be introduced in the lung region due to the low-dose imaging and, or postreconstruction denoising, no more than 40% low-dose imaging is recommended if no denoising approach is supposed to be applied. Nevertheless, the application of the bilateral filter to the 20% low-dose CT images led to a similar image quality of the 60% low-dose images without applying any denoising filters. Dose reduction beyond 20% is not recommended for COVID-19 patients as the quantitative bias as well as image artifact would impair the correct diagnosis or grading of COVID-19 disease.

Conclusion

This work set out to investigate low-dose CT imaging for COVID-19 patients, and in particular, to what extent acquisition dose could be reduced with no significant quantitative bias or image artifact. For this purpose, different low-dose CT imaging, namely 60%, 40%, 20%, and 10% of the standard dose, were simulated and quantitatively assessed before and after applying the common denoising techniques. Dose reduction beyond 20% introduced considerable quantitative bias as well as image artifact, which may skew the correct diagnosis or grading of COVID-19 infection in the lung region; thus, dose reduction beyond 20% is not recommended for COVID-19 patients. The quantitative evaluation of the low-dose CT images indicated the superior performance of the bilateral filter, particularly in the lung region compared to the Gaussian and median filters, which resulted in <5% quantitative bias in the lung for the 20% dose images.

Table 4: Mean±standard deviation of peak signal-to-noise ratio, structural similarity index measure, root mean square error, and bias calculated for the different low-dose computed tomography after application of the bilateral filter within the whole body, lung, and whole body without lung across 49 patients

	SSIM	PSNR	RMSE	Bias
60% dose				
Whole body	0.73±0.09	31.75±1.80	83.54±7.31	−0.36±0.30
Lung	0.93±0.01	27.45±1.90	79.23±14.84	0.20±0.31
Whole body without lung	0.80±0.08	31.75±1.83	82.27±8.66	−0.25±0.26
40% dose				
Whole body	0.70±0.10	30.80±1.83	93.22±7.65	−0.33±0.46
Lung	0.92±0.02	26.92±1.71	83.95±13.61	−0.56±0.55
Whole body without lung	0.75±0.09	30.51±1.82	96.46±9.05	−0.54±0.45
20% dose				
Whole body	0.61±0.10	28.85±1.85	116.82±11.52	0.40±0.90
Lung	0.91±0.02	25.38±1.68	100.21±16.47	−0.21±1.20
Whole body without lung	0.71±0.10	27.73±1.88	132.94±12.93	−0.47±0.99
10% dose				
Whole body	0.54±0.11	26.41±2.01	160.79±27.35	2.83±1.75
Lung	0.89±0.02	23.41±2.04	127.06±28.76	4.91±3.21
Whole body without lung	0.65±0.10	25.01±1.91	182.41±24.83	1.54±1.81

SSIM – Structural similarity index measure; PSNR – Peak signal-to-noise ratio; RMSE – Root mean square error

Financial support and sponsorship

The authors would like to thank the University of Isfahan and the the Avicenna Center of Excellence (ACE) for their support. The grant of this research have been registered under grant number of 9912011 in the University of Isfahan.

Conflicts of interest

There are no conflicts of interest.

References

1. Wu Z, McGoogan JM. Characteristics of and important lessons from the coronavirus disease 2019 (COVID-19) outbreak in China: Summary of a Report of 72 314 Cases from the Chinese Center for Disease Control and Prevention. JAMA 2020;323:1239-42.
2. World Health Organization. Coronavirus Disease (COVID-19) Pandemic; November 07, 2021.
3. Lai CC, Shih TP, Ko WC, Tang HJ, Hsueh PR. Severe acute respiratory syndrome coronavirus 2 (SARS-CoV-2) and coronavirus disease-2019 (COVID-19): The epidemic and the challenges. Int J Antimicrob Agents 2020;55:105924.
4. Katal S, Aghaghazvini L, Gholamrezanezhad A. Chest-CT findings of COVID-19 in patients with pre-existing malignancies; a pictorial review. Clin Imaging 2020;67:121-9.
5. Tang YW, Schmitz JE, Persing DH, Stratton CW. Laboratory diagnosis of COVID-19: Current issues and challenges. J Clin Microbiol 2020;58:e00512-20.
6. Fang Y, Zhang H, Xie J, Lin M, Ying L, Pang P, *et al.* Sensitivity of chest CT for COVID-19: Comparison to RT-PCR. Radiology 2020;296:E115-7.
7. Bao C, Liu X, Zhang H, Li Y, Liu J. Coronavirus disease 2019 (COVID-19) CT findings: A systematic review and meta-analysis. J Am Coll Radiol 2020;17:701-9.
8. Kim H, Hong H, Yoon SH. Diagnostic performance of CT and reverse transcriptase polymerase chain reaction for coronavirus disease 2019: A meta-analysis. Radiology 2020;296:E145-55.
9. Gholizadeh-Ansari M, Alirezaie J, Babyn P. Deep learning for low-dose CT denoising using perceptual loss and edge detection layer. J Digit Imaging 2019;33:504-15.
10. Arabi H, Kamali-Asl AR, Ay MR, Zaidi H. Monte Carlo-based assessment of the trade-off between spatial resolution, field-of-view and scattered radiation in the variable resolution X-ray CT scanner. Med Phys 2015;31:510-6.
11. Arabi H, Asl AR, Ay MR, Zaidi H. Novel detector design for reducing intercell x-ray cross-talk in the variable resolution x-ray CT scanner: A Monte Carlo study. Med Phys 2011;38:1389-96.
12. Lohrabian V, Kamali-Asl AR, Arabi H, Mamashi F, Hemmati HR, Zaidi H. Design and construction of a variable resolution cone-beam small animal mini-CT prototype for *in vivo* studies. Radiat Phys Chem 2019;162:199-207.
13. Safdarian N, Dabanloo NJ. Detection and classification of COVID-19 by lungs computed tomography scan image processing using intelligence algorithm. J Med Signals Sens 2021;11:274-84.
14. Karimian A, Yazdani S, Askari MA. Reducing the absorbed dose in analogue radiography of infant chest images by improving the image quality, using image processing techniques. Radiat Prot Dosimetry 2011;147:176-9.
15. Donya M, Radford M, ElGuindy A, Firmin D, Yacoub MH. Radiation in medicine: Origins, risks and aspirations. Glob Cardiol Sci Pract 2014;2014:437-48.
16. Sakane H, Ishida M, Shi L, Fukumoto W, Sakai C, Miyata Y, *et al.* Biological effects of low-dose chest CT on chromosomal DNA. Radiology 2020;295:439-45.
17. Arabi H, Kamali-Asl AR, editors. Feasibility Study of a New Approach for Reducing of Partial Volume Averaging Artifact in CT Scanner. 17th Iranian Conference of Biomedical Engineering, 3-4 November, 2010; 2010.
18. Arabi H, Kamali-Asl AR, Aghamiri SM. The effect of focal spot size on the spatial resolution of variable resolution X-ray CT scanner. Int J Radiat Res 2010;8:37-43.
19. Rehani MM, Szczykutowicz TP, Zaidi H. CT is still not a low-dose imaging modality. Med Phys 2020;47:293-6.
20. Hsieh J, Nett B, Yu Z, Sauer K, Thibault JB, Bouman CA. Recent advances in CT image reconstruction. Curr Radiol Rep 2013;1:39-51.
21. Shiri I, Akhavanallaf A, Sanaat A, Salimi Y, Askari D, Mansouri Z, *et al.* Ultra-low-dose chest CT imaging of COVID-19 patients using a deep residual neural network. Eur Radiol 2021;31:1420-31.
22. Arabi H, Zaidi H. Improvement of image quality in PET using post-reconstruction hybrid spatial-frequency domain filtering. Phys Med Biol 2018;63:215010.
23. Fadaee M, Shamsi M, Saberkari H, Sedaaghi MH. Computed tomography images de-noising using a novel two stage adaptive algorithm. J Med Signals Sens 2015;5:220-9.
24. Ehman EC, Yu L, Manduca A, Hara AK, Shiung MM, Jondal D, *et al.* Methods for clinical evaluation of noise reduction techniques in abdominopelvic CT. Radiographics

2014;34:849-62.
25. Sanaat A, Arabi H, Mainta I, Garibotto V, Zaidi H. Projection space implementation of deep learning-guided low-dose brain PET imaging improves performance over implementation in image space. J Nucl Med 2020;61:1388-96.
26. Wang J, Lu H, Liang Z, Eremina D, Zhang G, Wang S, *et al.* An experimental study on the noise properties of x-ray CT sinogram data in Radon space. Phys Med Biol 2008;53:3327-41.
27. Zhang H, Wang J, Zeng D, Tao X, Ma J. Regularization strategies in statistical image reconstruction of low-dose x-ray CT: A review. Med Phys 2018;45:e886-907.
28. Zeraatkar N, Sajedi S, Farahani MH, Arabi H, Sarkar S, Ghafarian P, *et al.* Resolution-recovery-embedded image reconstruction for a high-resolution animal SPECT system. Phys Med 2014;30:774-81.
29. Arabi H, Zaidi H. Spatially guided nonlocal mean approach for denoising of PET images. Med Phys 2020;47:1656-69.
30. Wang J, Li T, Lu H, Liang Z. Penalized weighted least-squares approach to sinogram noise reduction and image reconstruction for low-dose X-ray computed tomography. IEEE Trans Med Imaging 2006;25:1272-83.
31. Thibault JB, Sauer KD, Bouman CA, Hsieh J. A three-dimensional statistical approach to improved image quality for multislice helical CT. Med Phys 2007;34:4526-44.
32. Karimi D, Deman P, Ward R, Ford N. A sinogram denoising algorithm for low-dose computed tomography. BMC Med Imaging 2016;16:11.
33. Arabi H, Zaidi H. Non-local mean denoising using multiple PET reconstructions. Ann Nucl Med 2021;35:176-86.
34. Manduca A, Yu L, Trzasko JD, Khaylova N, Kofler JM, McCollough CM, *et al.* Projection space denoising with bilateral filtering and CT noise modeling for dose reduction in CT. Med Phys 2009;36:4911-9.
35. Hilts M, Duzenli C. Image filtering for improved dose resolution in CT polymer gel dosimetry. Med Phys 2004;31:39-49.
36. Pickhardt PJ, Lubner MG, Kim DH, Tang J, Ruma JA, del Rio AM, *et al.* Abdominal CT with model-based iterative reconstruction (MBIR): Initial results of a prospective trial comparing ultralow-dose with standard-dose imaging. AJR Am J Roentgenol 2012;199:1266-74.
37. Fletcher JG, Grant KL, Fidler JL, Shiung M, Yu L, Wang J, *et al.* Validation of dual-source single-tube reconstruction as a method to obtain half-dose images to evaluate radiation dose and noise reduction: Phantom and human assessment using CT colonography and sinogram-affirmed iterative reconstruction (SAFIRE). J Comput Assist Tomogr 2012;36:560-9.
38. Sadri AR, Zekri M, Sadri S, Gheissari N. Impulse noise cancellation of medical images using wavelet networks and median filters. J Med Signals Sens 2012;2:25-37.
39. Kim BG, Kang SH, Park CR, Jeong HW, Lee Y. Noise level and similarity analysis for computed tomographic thoracic image with fast non-local means denoising algorithm. Appl Sci 2020;10:7455.
40. Dang N, Thanh H. A review on CT and X-Ray images denoising methods. Informatica 2018;43:151-9.
41. Arabi H, Zaidi H. Applications of artificial intelligence and deep learning in molecular imaging and radiotherapy. Eur J Hybrid Imaging 2020;4:17.
42. Arabi H, Dowling JA, Burgos N, Han X, Greer PB, Koutsouvelis N, *et al*. Comparative study of algorithms for synthetic CT generation from MRI: Consequences for MRI-guided radiation planning in the pelvic region. Med Phys 2018;45:5218-33.
43. Arabi H, Bortolin K, Ginovart N, Garibotto V, Zaidi H. Deep learning-guided joint attenuation and scatter correction in multitracer neuroimaging studies. Hum Brain Mapp 2020;41:3667-79.
44. Bahrami A, Karimian A, Arabi H. Comparison of different deep learning architectures for synthetic CT generation from MR images. Phys Med 2021;90:99-107.
45. Bahrami A, Karimian A, Fatemizadeh E, Arabi H, Zaidi H. A new deep convolutional neural network design with efficient learning capability: Application to CT image synthesis from MRI. Med Phys 2020;47:5158-71.
46. Alnaser A, Gong B, Moeller K. Evaluation of open-source software for the lung segmentation. Curr Direct Biomed Eng 2016;2:515-8.
47. Wang X, Zamyatin A, Shi D, editors. Dose Reduction Potential with Photon Counting Computed Tomography. Medical Imaging 2012: Physics of Medical Imaging; 2012: International Society for Optics and Photonics; 2012.
48. Park J, Han JH, Lee BU. Performance of bilateral filtering on Gaussian noise. J Electron Imaging 2014;23:043024.
49. Slovis TL. Children, computed tomography radiation dose, and the As Low As Reasonably Achievable (ALARA) concept. Pediatrics 2003;112:971-2.
50. Thanh D, Surya P. A review on CT and X-ray images denoising methods. Informatica 2019;43:151-9.